RCS measurements and ISAR images of small UAVs

Feature Article:

DOI. No. 10.1109/MAES.2017.160167

RCS Measurements and ISAR Images of Small UAVs

***Massimiliano Pieraccini, Lapo Miccinesi, Neda Rojhani*, University of Florence, Firenze, Italy**

INTRODUCTION

Currently small unmanned aerial vehicles (UAV) pose a serious threat for the safety of flights. The Aviation Authorities are dealing with this issue worldwide. Recently (October 2015), the U.S. Federal Aviation Administration gave permission to test antidrone technology that would counter rogue drones flying within a five-mile radius of selected airports [1]. Airport safety is only one of the problems that the increasing number of UAVs can pose. A critical issue is to prevent UAVs being used for terrorist attacks, espionage, or other malicious activities against sites with critical infrastructure. Last but not least, UAVs flying in private area pose privacy concerns [2].

Radar could be the technology of choice for detecting them, but standard air defense is ill-prepared for UAV detection: UAVs are low-velocity aircraft with a very weak radar signature. Despite this, the scientific literature lacks detailed experimental studies on the radar cross section (RCS) of small UAVs [3], [4], [5], especially for quadcopters that are the most popular civil UAVs. Therefore, the first aim of this article is to carry out RCS measurements of small drones, in particular of a toy drone and a professional quadcopter.

The RCS measurements give global information on a target, but they do not provide information on which features are mainly responsible for the radar response. Inverse Synthetic Aperture Radar (ISAR) [6], [7], [8] processing provides just this kind of information.

THE MEASUREMENT EQUIPMENT

A sketch of the measurement equipment is shown in Figure 1. A vector network analyzer (HP 8720A) operates as Continuous Wave Step Frequency transceiver. It is linked through microwave cables to a radar front-end held on a tripod.

The front-end is provided with a pair of single-pole double-throw switches that provides a direct path (through a −40 dB attenuator) between the transmitter and the receiver in order to perform calibrated measurements. The antennas are two equal horns linearly polarized, with a rectangular aperture 5.5 cm × 7.5 cm, designed for operating in the 8–12 GHz band. Their measured efficiency has been $\eta = 0.446 \pm 0.040$.

As shown in Figure 1, the target under test was positioned on a platform that can be rotated step-by-step. For each k angular position, the equipment carried out a sweep of N_f frequencies between 8 GHz and 12 GHz with the switches connected to antennas and a second sweep with the switches connected to the attenuator (−40 dB). The ratio, frequency by frequency, gives a calibrated measurement. A complete acquisition is a matrix of complex numbers $E_{i,k}$, with i index relative to the frequency and k index relative to the angular position. After the radar acquisition, the target under test was removed and a single frequency sweep was performed. This later acquisition (called *empty room*) was subtracted to each column of matrix $E_{i,k}$ (*background removal*).

Before the measurements session of the targets under test, the equipment was calibrated using three known targets positioned at 17 m in front of the antennas: a metallic sphere of 0.45 m diameter, a corner reflector of 0.30 m side, and a second corner reflector of 0.50 m side. From the radar equation [9], the RCS (σ) can be obtained from the following equation:

$$\sigma_k = \frac{\gamma}{4\pi}\left(\frac{4\pi F R_0^2 \lambda}{\alpha \eta A} u_k\right)^2 \tag{1}$$

where A is the physical area of RX antenna, η is the antenna efficiency, λ wavelength, u_k is peak amplitude of the inverse fast Fourier transform (IFFT) (along the i-index) of $E_{i,k}$, γ power attenuation of the calibration path (−40 dB), and F padding factor of IFFT. The α factor takes into account the decreasing of the peak

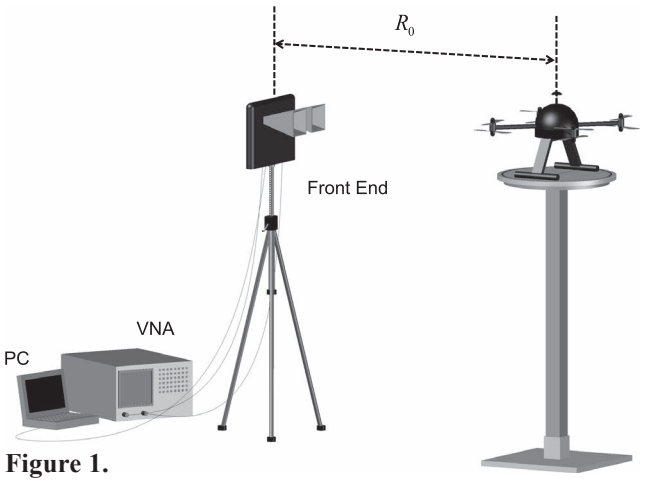

Figure 1.
Sketch of the measurement equipment.

Authors' address: Department of Information Engineering (DINFO), University of Florence, Via Santa Marta, 3, Firenze, Italy, 50139, E-mail: (massimiliano.pieraccini@unifi.it).
Manuscript received August 4, 2016, revised November 23, 2016, and ready for publication February 6, 2017.
Review handled by D. O'Hagan.
0885/8985/17/$26.00 © 2017 IEEE

amplitude due to the frequency windowing: $\alpha = 0.5442$ in the case of a Kaiser window with $\beta = 5$.

THE UAVS UNDER TEST

As a representative toy drone we selected a SYMA X5SC-1 quadcopter (Figure 2). Although it is provided with a 2.0 Megapixel camera, it is intended to be a low-cost toy not for professional use. It is powered by a built-in 500 mAh Li-Poli battery. The distance from the motors is 16 cm. Their height from the ground is 4.5 cm. The frame and the blades are made of plastic material.

We selected a NT4Contra quadcopter, manufactured by AirVision (Figure 6), as representative professional UAV. It has four pairs of engines with counter-rotating blades. The frame is made of carbon. It is powered by two 4,600 mAh Li-Poli batteries housed in the legs. Below the head there is a dock for a camera (not provided). The distance from the motors is 36 cm. The height of the motors from ground is 22 cm (Figure 3).

RCS MEASUREMENTS

The SYMA quadcopter was placed over the platform and a complete measurement with antennas in vertical polarization was carried out. The distance between the antennas and the rotation center was 156 cm. The angular step was 1 deg. By using a Kaiser window with $\beta = 5$, a 500 MHz bandwidth gives a Full Width at Half Maximum (FWHM) equal to 0.54 m (larger than the size of the quadcopter). The measured angular pattern of RCS is shown in Figure 4. The largest values are in correspondence of the four motors. The measured main value of the RCS was 0.0312 m^2.

By rotating the antennas, the RCS of the SYMA quadcopter was also measured in horizontal polarization. The obtained main value has been 0.0229 m^2. There are not substantial differences with respect to the RCS pattern in vertical polarization.

The same measurements have been performed with the AirVision quadcopter. The measured angular pattern of RCS in vertical polarization is shown in Figure 5. For this quadcopter, the largest RCS values are in front and back. The main value is 0.271 m^2.

By rotating the antennas, the RCS of AirVision quadcopter was also measured in horizontal polarization. The obtained main value has been 0.2759 m^2. There are no substantial differences between the RCS patterns in horizontal and vertical polarizations. Table 1 summarizes the obtained results.

Just a note about the distance between antenna and target: for both the UAVs it was 156 cm. The RCS of a target should be measured in the far field both of antenna and of target. The first

Figure 2.
SYMA quadcopter.

Figure 3.
AirVision quadcopter.

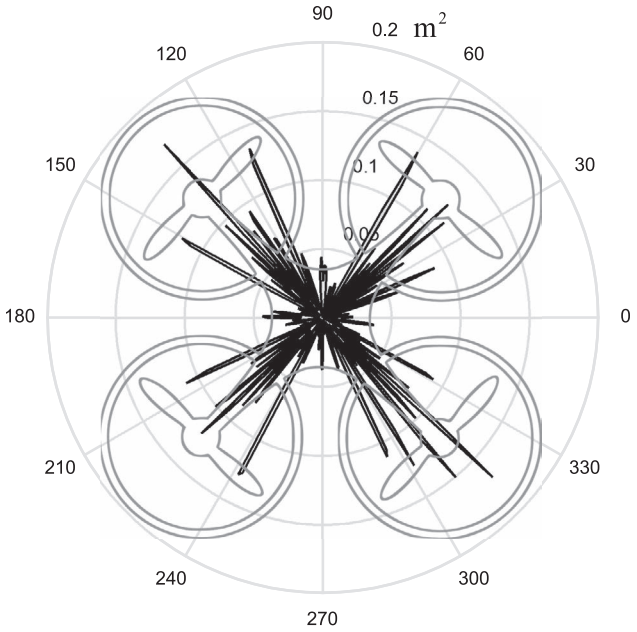

Figure 4.
RCS angular pattern of SYMA quadcopter.

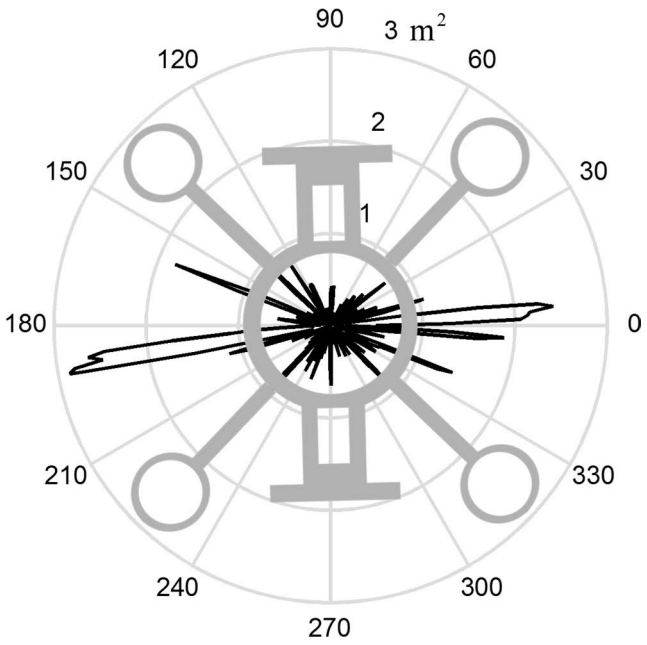

Figure 5.
RCS distribution of AirVision quadcopter.

Table 1.

Measured RCS		
	Vertical Polarization	**Horizontal Polarization**
SYMA X5SC-1	0.0312 m²	0.0229 m²
AIRVISION NT4CONTRAS	0.271 m²	0.276 m²

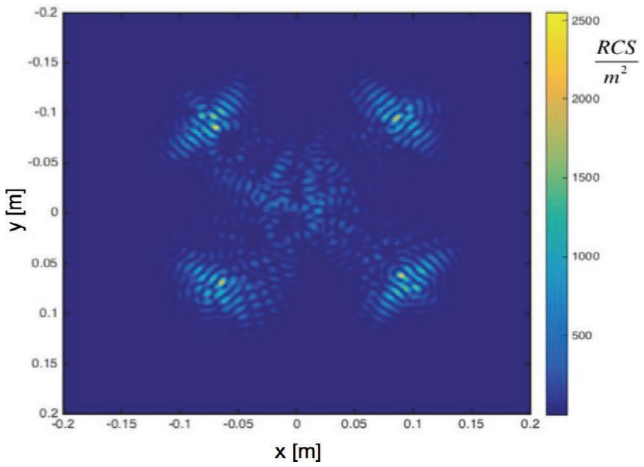

Figure 6.
2D-ISAR image of SYMA quadcopter.

condition is always respected, But the latter condition is not respected in the measurements with the bigger UAV (AIRVISION NT4CONTRAS). Fortunately this is not a serious issue, as suitable algorithms have been developed for transforming near-field data in far-field data [10], [11]. In particular, we used the well-known algorithm by Mensa and Vaccaro as described in [11].

ISAR PROCESSING

The ISAR processing allows to obtain a two-dimensional (2D) (or even a three-dimensional (3D)) image of the RCS distribution. It is particularly useful to identify the features of the target that contribute most to the radar signal. The basic idea of ISAR is to exploit the spatial diversity of data acquired for focusing a high-resolution image.

Using the above-mentioned equipment, the result of a measurement session is a matrix $N_f \times N_p$ of complex numbers:

$$E_{i,k} = I_{i,k} + jQ_{i,k} \tag{2}$$

where $I_{i,k}$ and $Q_{i,k}$ are the in-phase and the quadrature components acquired at *i*th frequency ($1 < i < N_f$) and at the *k*th angular position ($1 < k < N_p$). The basic formula for focusing in a generic point identified by the coordinate (x, y, z) is [6]:

$$I(x,y,z) = \sum_{i,k} E_{i,k} e^{j\frac{4\pi}{c} f_i R_k(x,y)} \tag{3}$$

where R_k (x, y, z) is the distance between the image-point (x, y, z) and the *k*th angular position of the antenna. Equation (8) is computationally very heavy, but several faster algorithms have been developed [6], [7], [8].

2D ISAR IMAGES

The SYMA quadcopter was placed on the platform as shown in Figure 1. The antennas operated in vertical polarization. The distance between the antennas and the rotation center was 202 cm. The angular step was 1 deg. The bandwidth was B = 4GHz; that

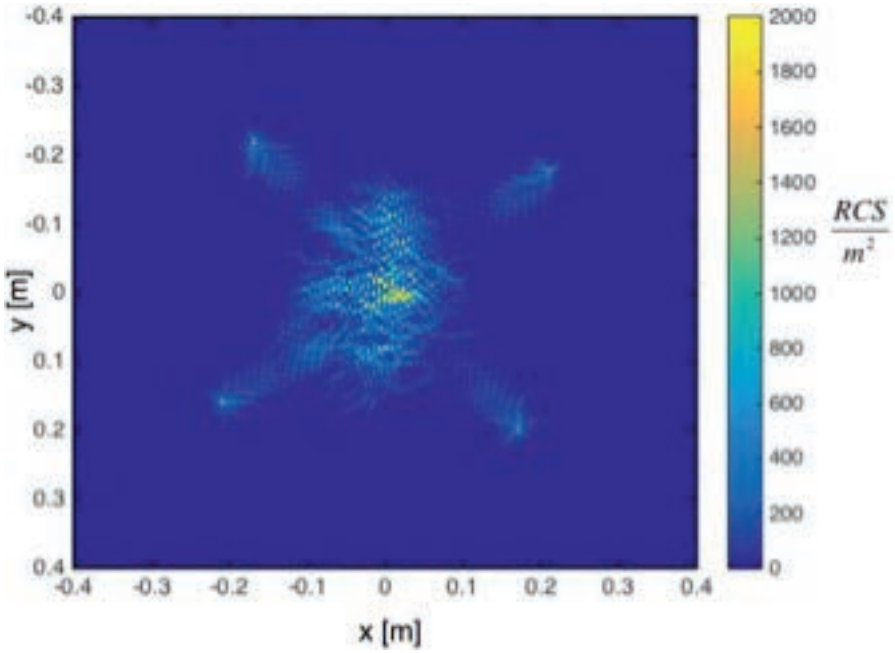

Figure 7.
2D-ISAR image AirVision quadcopter.

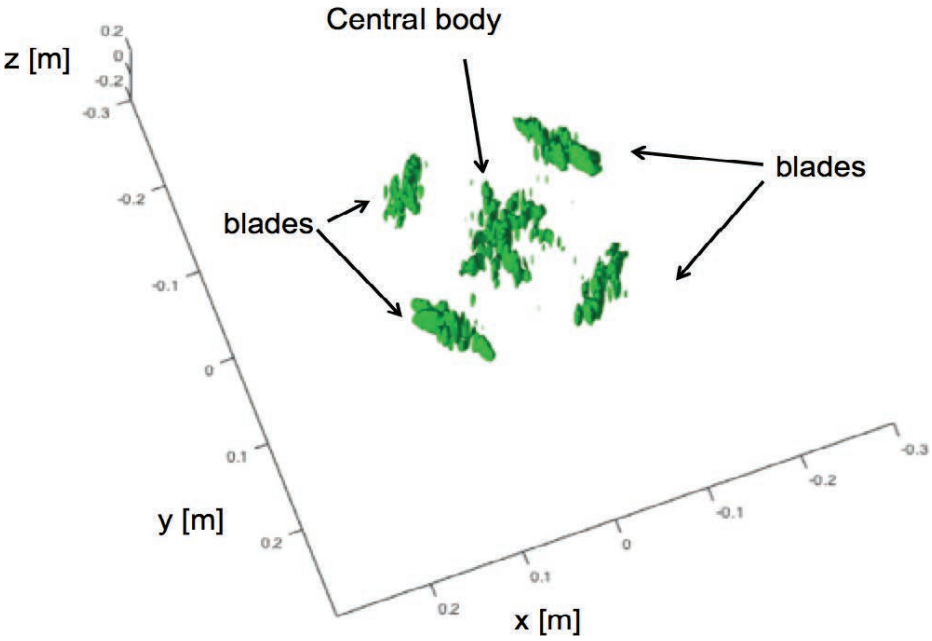

Figure 8.
3D-ISAR image of SYMA X5SC-1 quadcopter.

gives a FWHM in range equal to 0.136 m, using a Kaiser window with $\beta = 5$. The obtained RCS image is shown in Figure 6. The shape of a quadcopter can be easily recognized. The four motors give a clear, high signal.

The same measurements were performed with the AirVision quadcopter. The obtained RCS image is shown in Figure 7. Also in this case the shape of quadcopter can be easily recognized but, unlike SYNA quadcopter, the motors do not give the highest RCS signal.

3D ISAR IMAGES

The focusing formula in (3) can be applied to the 3D case by carrying out radar measurement at different height of the rotation plane. With this aim, the height of the platform was varied of 18 cm at step of 1.0 cm. The contour plot of the obtained 3D image of the smaller UAV is shown in Figure 8. The four blades are clearly recognizable, as well as the central body.

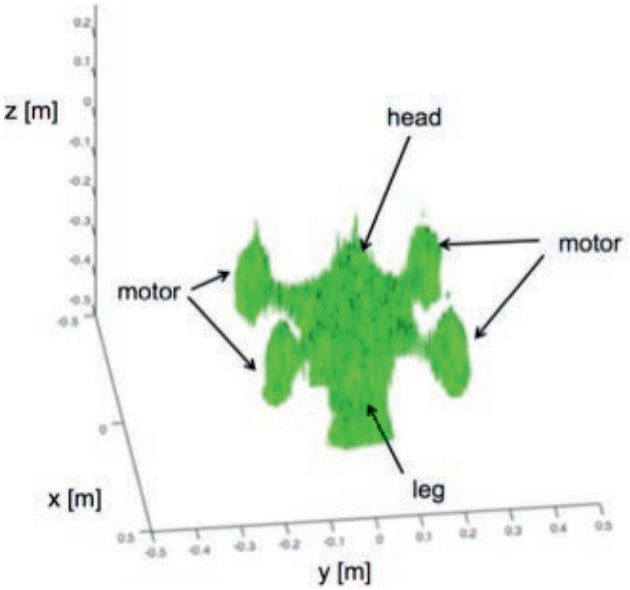

Figure 9.
3D-ISAR image of AirVision quadcopter.

Figure 9 shows the contour plot of the 3D image of the bigger UAV. The height of the platform was varied of 26 cm at step of 1.0 cm. The shape of the motors (a couple of motors in line to be more precise) are clearly recognizable, as well as the legs and the head of quadcopter.

Finally, by using the whole measurement set (9,270 single acquisitions), we calculated the RCS statistical distribution, as shown in Figure 10, that resulted in very good agreement with the well-known Swerling Case I distribution [12]:

$$p(\sigma) = \frac{1}{\bar{\sigma}} e^{-\frac{\sigma}{\bar{\sigma}}} \tag{4}$$

where $\bar{\sigma}$ is the mean value of RCS. Indeed the χ^2 goodness-of-fit test rejected the null hypothesis at the 1% significance level.

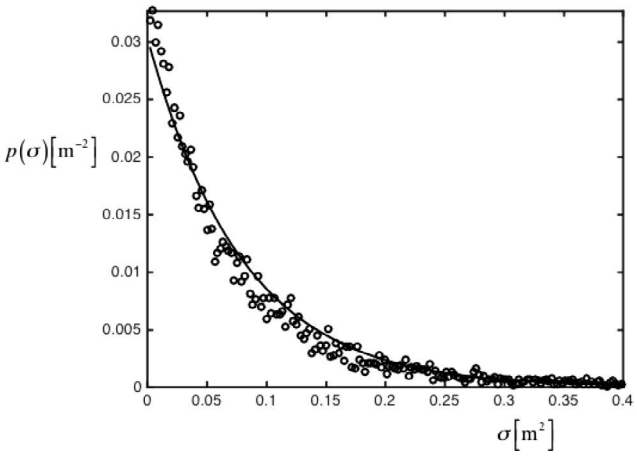

Figure 10.
RCS distribution of AirVision quadcopter using the whole measurement set for 3D ISAR. The full line is the Swerling distribution.

CONCLUSIONS

RCS measurement of a toy drone and a professional quadcopter has been carried out. A significant finding of this work is that Swerling distribution is in very good agreement with the RCS statistical distribution of the quadcopters we tested. This is not an obvious fact. Swerling Case I distribution was obtained in a very heuristic hypothesis (a random set of equal scatters on a planar surface) and—at least in the open literature—it has never been tested with quadcopters or other small UAVs. Another finding that is worth mentioning is that mean RCS in vertical and horizontal polarization are nearly equal. ◈

ACKNOWLEDGMENT

The authors are grateful to Prof. Alberto del Bimbo, director of MICC (Media Integration and Communication Center), who kindly made the AirVision quadcopter available all the necessary time to compile the RCS measurements.

REFERENCES

[1] CNN. http://edition.cnn.com/2015/10/07/politics/faa-anti-drone-technology/, Oct. 8, 2015.

[2] The New York Times. http://www.nytimes.com/2016/01/10/opinion/sunday/drone-regulations-should-focus-on-safety-and-privacy.html?_r=0, Jan. 9, 2016.

[3] To, L., Bati, A., and Hilliard, D. Radar cross section measurements of small unmanned air vehicle systems in non-cooperative field environments. In *Proceedings of the IEEE 2009 3rd European Conference on Antennas and Propagation*, Mar. 2009, 3637–3641.

[4] Altin, N., and Yazgan, E. The calculation of back scattering field of unmanned air vehicle. In *Proceedings of PIERS*, Beijing, China, Mar. 23–27, 2009, 1460–1463.

[5] Ritchie, M. A., Fioranelli, F., Griffith, H., and Torvik, B. Micro-drone RCS analysis. In *Proceedings of the International Conference on RADAR*, Johannesburg, South Africa, Oct. 2015.

[6] Mensa, D. L. *High Resolution Radar Cross-Section Imaging* (2nd ed.). Artech House, 1991.

[7] Fortuny, J. An efficient 3-D near-field ISAR algorithm. *IEEE Transactions on Aerospace and Electronic Systems*, Vol. 34, 4 (1998), 1261–1270.

[8] Mayhan, J. T., Burrows, M. L., Cuomo, K. M., and Piou, J. E. High resolution 3D "snapshot" ISAR imaging and feature extraction. *IEEE Transactions on Aerospace and Electronic Systems*, Vol. 37, 2 (2001), 630–642.

[9] Skolnik, M. I. *Radar Handbook*. McGraw-Hill, 2008.

[10] Yaghjw, A. D. An overview of near-field antenna measurements. *IEEE Transactions on Antennas and Propagation*, Vol. AP-34, 1 (Jan. 1986).

[11] Gao, C., Chen, J. W., Jin, M., and Bai, Y. A method for predicting far field radar cross-section from near field measurements on cylindrical scanning mode. In *Proceedings of PIERS*, Guangzhou, China, Aug. 25–28, 2014, 1140–1145.

[12] Swerling, P. Probability of detection for some additional fluctuating target cases. Aerospace Corp., Los Angeles, CA, Rep. TOR-669 (9099), Mar. 14, 1966. Reprinted in *IEEE Transactions on Aerospace and Electronic Systems*, Vol. 33, 2 (1997), 698–709.

IEEE

Aerospace and Electronic SYSTEMS magazine

September 2017
ISSN 0885-8985
Volume 32 Number 9

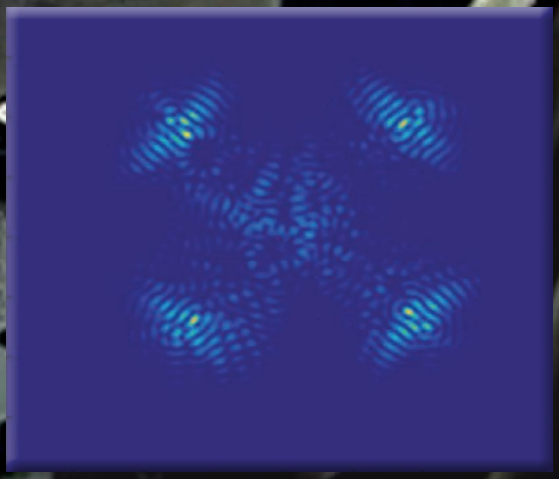

AESS

IEEE

This Month's Covers....

Front and Back Cover Background: The cockpit and pilots of an Osprey that flies in both airplane and helicopter mode. Marine Lt. Col. Kevin Gross, V-22 Osprey Integrated Test Team's Government Flight Test Director, seated left, and Marine Maj. Gen. Jim Amos, Commanding General 3rd Marine Air Wing, pose for a photo while making preparations for the General's aircraft familiarization flight. U.S. Navy photo (Patuxent River, MD, USA, January 9, 2004) by Randy Teufel (RELEASED).

Front Cover: Upper inset: An Image called "Quadcopter" by Jens Vanhooydonck (Zelf gemaakt) CC BY-SA 3.0 (https://creativecommons.org/licenses/by-sa/3.0)], via Wikimedia Commons (2013). **Lower inset:** A 2D-ISAR image of a SYMA quadcopter. This graphic appears in Figure 6 of the article, "RCS Measurements and ISAR Images of Small UAVs," by Pieraccini, Miccinesi, and Rojhini in this issue on pages 28-32. Unlike the Osprey whose cockpit and pilots are pictured in the background, the vehicles pictured in both insets are unmanned.

Back Cover: Upper inset: 2D-ISAR image of an AirVision quadcopter. This graphic appears in Figure 7 in the article, "*RCS Measurements and ISAR Images of Small UAVs*," by Pieraccini et al. in this issue on pages 28-32. **Lower inset:** Photo of an Aeryon Scout UAV in flight. By Dkroetsch (Own work) [Public domain], via Wikimedia Commons. As on the front cover, the inset vehicles are both unmanned, different from the Osprey whose cockpit and human pilots are pictured in the background photo.

IEEE AESS Society

The IEEE Aerospace and Electronic Systems Society is a society, within the framework of the IEEE, of members with professional interests in the organization, design, development, integration and operation of complex systems for space, air, ocean, or ground environments. These systems include, but are not limited to, navigation, avionics, spacecraft, aerospace power, mobile electric power & electronics, military, law enforcement, radar, sonar, telemetry, defense, transportation, automatic test, simulators, and command & control. Many members are concerned with the practice of system engineering. All members of the IEEE are eligible for membership in the Society and receive the Society magazine *Systems* upon payment of the annual Society membership fee. The *Transactions* are unbundled, online only, and available at an additional fee. For information on joining, write to the IEEE at the address below. Member copies of publications are for personal use only.

IEEE AEROSPACE AND ELECTRONIC SYSTEMS MAGAZINE® (ISSN 0885-8985; USPS 212-660) is published monthly by the Institute of Electrical and Electronics Engineers, Inc. Responsibility for the contents rests upon the authors and not upon the IEEE, the Society/Council, or its members. IEEE Corporate Office: Three Park Avenue, 17th Floor, New York, NY 10016-5997, USA. IEEE Operations Center: 445 Hoes Lane, P.O. Box 1331, Piscataway, NJ 08855-4141, USA. NJ Telephone: 732-981-0060. Price/Publication Information: Individual copies: IEEE member $20.00 (first copy only), nonmembers $63.00 per copy. (Postage and handling charge not included.) Member and nonmember subscription prices available upon request. Available in microfiche and microfilm.

Periodicals postage paid at New York, NY, and at additional mailing offices. Postmaster: Send address changes to IEEE Aerospace and Electronic Systems Magazine, IEEE, 445 Hoes Lane, P.O. Box 1331, Piscataway, NJ 08855-4141. GST Registration No. 125634188. CPC Sales Agreement #40013087. Return undeliverable Canada addresses to: Pitney Bowes IMEX, P.O. Box 4332, Stanton Road, Toronto, ON M5W 3J4, Canada. Printed in the United States of America.